COMPUTER METHODS AND PROGRAMS IN BIOMEDICINE 123 (2016) 43–53

journal homepage: www.intl.elsevierhealth.com/journals/cmpb

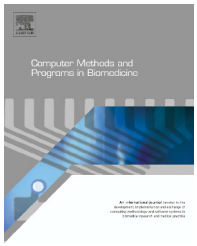

A novel breast ultrasound image segmentation algorithm based on neutrosophic similarity score and level set

Yanhui Guo[a,*], *Abdulkadir Şengür*[b], *Jia-Wei Tian*[c]

[a] *Department of Computer Science, University of Illinois at Springfield, Springfield, IL, USA*
[b] *Department of Electric and Electronics Engineering, Technology Faculty, Firat University, Elazig, Turkey*
[c] *Department of Ultrasound, Second Affiliated Hospital of Harbin Medical, Harbin, Heilongjiang, China*

ARTICLE INFO

Article history:
Received 23 April 2015
Received in revised form
2 September 2015
Accepted 8 September 2015

Keywords:
Breast ultrasound
Image segmentation
Neutrosophic set
Similarity score
Level set

ABSTRACT

Breast ultrasound (BUS) image segmentation is a challenging task due to the speckle noise, poor quality of the ultrasound images and size and location of the breast lesions. In this paper, we propose a new BUS image segmentation algorithm based on neutrosophic similarity score (NSS) and level set algorithm. At first, the input BUS image is transferred to the NS domain via three membership subsets *T*, *I* and *F*, and then, a similarity score NSS is defined and employed to measure the belonging degree to the true tumor region. Finally, the level set method is used to segment the tumor from the background tissue region in the NSS image. Experiments have been conducted on a variety of clinical BUS images. Several measurements are used to evaluate and compare the proposed method's performance. The experimental results demonstrate that the proposed method is able to segment the BUS images effectively and accurately.

1. Introduction

According to the statistics, breast cancer is one of the most common cancers among women and 232,670 new cases of invasive breast cancer were diagnosed among women in the US during 2014 [1], and an estimated 40,430 breast cancer deaths were expected in 2014 in US [2]. In statistics, breast cancer is indicated as the fifth most common causes of cancer death. However, these deaths can be reduced if cases are detected and treated early [2]. Breast ultrasound (BUS) is known to be a major imaging modality due to its low cost, real time and dynamical imaging, and without ionizing radiation [3]. BUS has also proved to be a suitable tool for large-scale screening addition to mammography in early detection of breast lesions [3]. However, clinical experience and expert knowledge are important factors to achieve accurate and fast diagnosis using BUS [3]. In other words, highly skilled physicians and radiologists are needed for interpretation of the BUS images.

In the last decades, several decision support systems have been proposed for helping the physicians in order to interpret the BUS images [4]. Generally these systems are using image processing and pattern recognition algorithms. Especially, image segmentation is vital to localize the lesions in these systems. However, speckle noise, poor quality and size and location of the breast lesions make this crucial step still challenging and difficult [3]. Up to now, a great number of

* *Corresponding author*. Tel.: +1 4352275882.
E-mail addresses: yanhui.guo@aggiusu.edu, yguo56@uis.edu (Y. Guo).

http://dx.doi.org/10.1016/j.cmpb.2015.09.007

automatic, semi-automatic and manual BUS image segmentation methods have been proposed.

According to the literature, the segmentation methods for BUS images are categorized into four groups [5]: histogram thresholding, active contour model, Markov random field, and neural network based methods.

Histogram thresholding is one of the widely used techniques for gray level image segmentation [6]. It is necessary to apply the histogram thresholding in BUS images segmentation. Although, the histogram thresholding methods are too simple and easy to implement, they generally do not perform well when the histograms are unimodal.

The active contour model, more widely known as snake [7], is a framework to delineate an object's contour from background, and an edge-based segmentation method. The snake model has been extensively used for BUS images [8,9]. A hybrid scheme combining region-based and boundary-based techniques was proposed for BUS image segmentation [10]. The seed points are automatically generated by empirical rules based formulation. The boundary points are then determined by region growing and directional gradient operation. Finally, a deformable model is employed for ROI segmentation. An active contour model based method is employed for BUS image segmentation [11]. The method is composed of two parts. ROI generation is followed by a ROI segmentation part. The authors reported improved accuracy according to their comparisons. Seed selection and subsequent contour initialization is carried out based on texture features and level set segmentation [12]. The deformation model based methods mostly handle only the regions of interest in the image (ROIs), not the whole image. In addition, automatically generating a suitable initial contour is very difficult, and the deformation procedure is very time-consuming.

Markov random field (MRF) model has been used for BUS image segmentation [13,14]. The MRF method provides a strong exploitation of the pixel correlations, and the segmentation results are further improved by the application of maximum a posteriori segmentation estimation scheme. However, it has complex iteration process and is time-consuming.

Classifier based methods [4,15,16] are popularly used in image segmentation. They generally convert the segmentation problem into classification decision based on a set of features. The BUS image segmentation method [4] is based on adaptive reference point classification algorithm, and tumor extraction is carried out based on a cost function, which is defined in terms of tumor's boundary and region information in both frequency and space domains. The classifier based methods are enough good but the algorithms would not perform well when the lesion was not compact and round-like. Moreover, the appropriate number of hidden units for the neural network was determined empirically. A ROI generation algorithm is combined multi-domain features to characterize the lesions in BUS image segmentation [17]. The lesion segmentation is carried out with neural network classifier. An object recognition based automatic lesion detection scheme is proposed for BUS images [18]. The method firstly filters the BUS image for speckle noise reduction and then a graph based segmentation method is applied to segment the image into a number of sub-regions. Tumor extraction is carried out based on object recognition methodology. A two stepped learning based algorithm is proposed for detection of breast tumor in ultrasound images [19]. The initial tumor localization is carried out with an AdaBoost classifier on Harr-like features and then the detected preliminary tumor regions are quantized using support vector machines. The segmentation is further completed with random walk method.

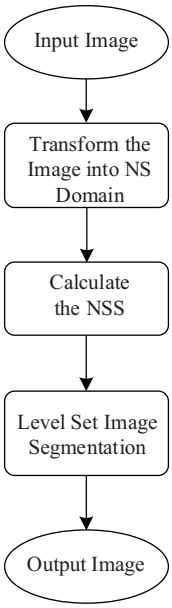

Fig. 1 – The flowchart of the proposed method.

Other methods were proposed recently for image segmentation. Pereira et al. [20] segmented breast masses on mammogram using multiple thresholding, wavelet transform and genetic algorithm. The method was quantitatively evaluated using the area overlap metric (AOM). The mean ± standard deviation value of AOM for the proposed method was 79.2 ± 8%. A marker-based watershed segmentation method [21] was proposed to segment background of X-ray images. The method includes image preprocessing, gradient computation, marker extraction, watershed segmentation from markers, region merging and background extraction. It yielded a dice coefficient of 0.964 ± 0.069.

Based on the reviewed literature, it is evident that image segmentation in BUS is still an open area for further research. In this paper, we propose a new breast ultrasound image segmentation algorithm based on neutrosophic similarity score and level set algorithm. A BUS image is represented in the neutrosophic set (NS) domain, and a neutrosophic similarity score (NSS) is defined and employed to measure the belonging degree to the true tumor. A level set method is finally used to segment the tumor from the background using the NSS value of the image. Experiments have been conducted on a variety of clinical BUS images. Several measurements are used to evaluate and compare the proposed method's performance. The experimental results demonstrate that the proposed method segments the BUS images effectively and accurately.

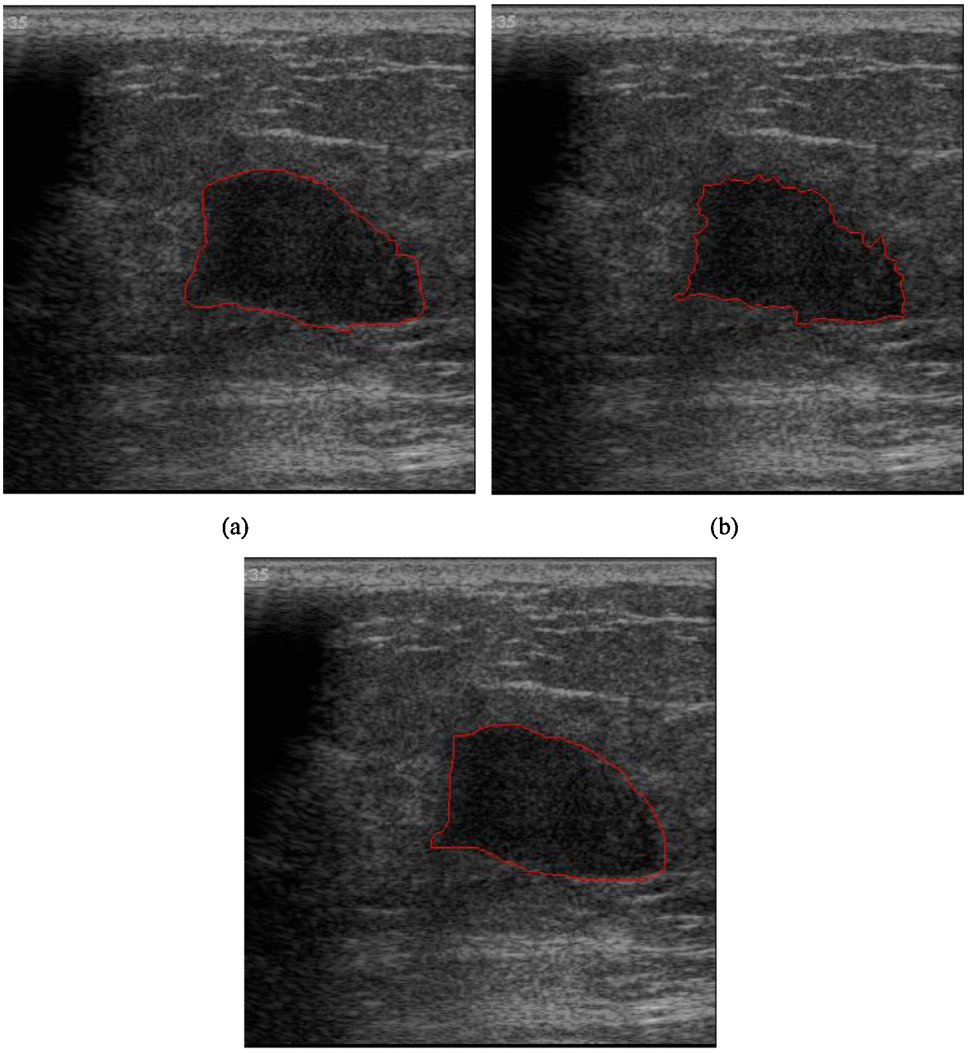

Fig. 2 – Example of tumor segmentation with different methods: (a) result by NSSLS, (b) result by FCMLS, and (c) radiologist's result.

The paper is organized as follows. Section 2 describes the proposed method. Section 3 discusses the experimental results and comparisons, and the conclusions are drawn in Section 4.

2. Proposed method

2.1. *Neutrosophic similarity score*

$A=\{A_1, A_2, \ldots, A_m\}$ and $C=\{C_1, C_2, \ldots, C_n\}$ are sets of alternatives and conditions in neutrosophic set (NS), respectively. The alternative A_i under the C_j condition is denoted as $\{T_{C_j}(A_i), I_{C_j}(A_i), F_{C_j}(A_i)\}/A_i$, where $T_{C_j}(A_i)$, $I_{C_j}(A_i)$ and $F_{C_j}(A_i)$ are the membership values to the true, indeterminate and false set at the C_j condition, respectively. An ideal alternative A^* is the best alternative denoted in NS as: $\{T^*_{C_j}(A_i), I^*_{C_j}(A_i), F^*_{C_j}(A_i)\}/A^*_i$.

A similarity score was defined to measure the similarity degree between two alternatives in NS [22] as:

$$S_{C_j}(A_m, A_n) = \frac{T_{C_j}(A_m)T_{C_j}(A_n) + I_{C_j}(A_m)I_{C_j}(A_n) + F_{C_j}(A_m)F_{C_j}(A_n)}{\sqrt{T^2_{C_j}(A_m) + I^2_{C_j}(A_m) + F^2_{C_j}(A_m)} \times \sqrt{T^2_{C_j}(A_n) + I^2_{C_j}(A_n) + F^2_{C_j}(A_n)}} \quad (1)$$

NS is specified into image domain as: in an image I_m, BP is a bright pixel set in I_m, and I_{NS} is the image neutrosophic set domain. A pixel $P(x, y)$ in I_m is mapped in NS domain: $P_{NS}(x, y)=\{T(x, y), I(x, y), F(x, y)\}$. $T(x, y)$, $I(x, y)$ and $F(x, y)$ represent memberships belonging to bright pixel set, indeterminate set and non-bright pixel set, respectively.

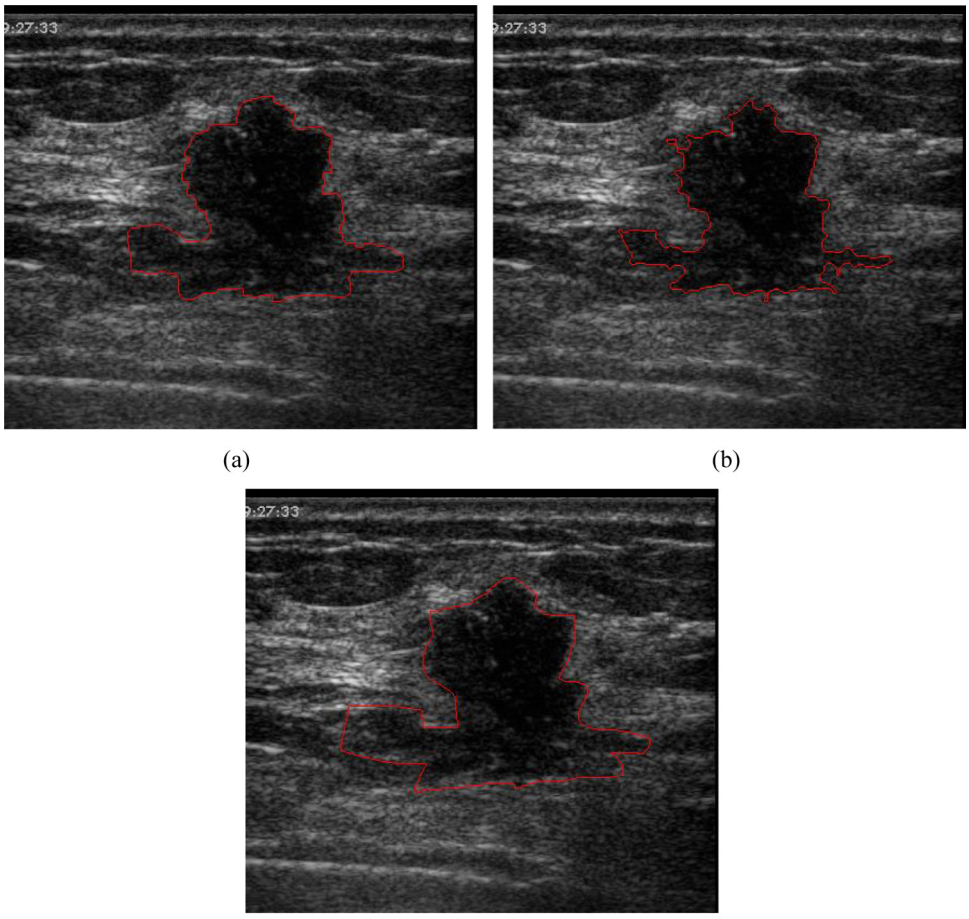

Fig. 3 – Example of tumor segmentation with different methods: (a) result by NSSLS, (b) result by FCMLS, and (c) radiologist's result.

The membership values can be defined under different conditions. At first, based on the intensity values, they are defined as:

$$T_{C_g}(x, y) = \frac{g(x, y) - g_{\min}}{g_{\max} - g_{\min}} \tag{2}$$

$$I_{C_g}(x, y) = \frac{Gd(x, y) - Gd_{\min}}{Gd_{\max} - Gd_{\min}} \tag{3}$$

$$F_{C_g}(x, y) = 1 - T_{C_g}(x, y) \tag{4}$$

where $g(x, y)$ and $Gd(x, y)$ are the intensity value and gradient magnitude at the position of (x, y) on the image.

To make the interpretation robust to noise, two new conditions, local mean intensity criterion C_m and local homogeneity criterion C_h, are used to map the pixel into NS domain. The neutrosophic values using the local mean intensity C_m is defined as:

$$T_{C_m}(x, y) = \frac{g_m(x, y) - g_{m\ \min}}{g_{m\max} - g_{m\min}} \tag{5}$$

$$g_m(x, y) = \frac{1}{w \times w} \sum_{m=x-w/2}^{x+w/2} \sum_{n=y-w/2}^{y+w/2} g(m, n) \tag{6}$$

$$I_{C_m}(x, y) = \frac{Gd_m(x, y) - Gd_{m\ \min}}{Gd_{m\max} - Gd_{m\min}} \tag{7}$$

$$F_{C_m}(x, y) = 1 - T_{C_m}(x, y) \tag{8}$$

where $g_m(x, y)$ and $Gd_m(x, y)$ are the intensity value and gradient magnitude value at the position of (x, y) on the image after mean filter processing.

The neutrosophic set under the local homogeneity condition C_h is also defined as:

$$T_{C_h}(x, y) = \frac{H(x, y) - H_{\min}}{H_{\max} - H_{\min}} \tag{9}$$

$$I_{C_h}(x, y) = \frac{Gd_h(x, y) - Gd_{h\ \min}}{Gd_{h\max} - Gd_{h\min}} \tag{10}$$

$$F_{C_h}(x, y) = 1 - T_{C_h}(x, y) \tag{11}$$

$$H(x, y) = \mathrm{TEM}(g(x, y)) \tag{12}$$

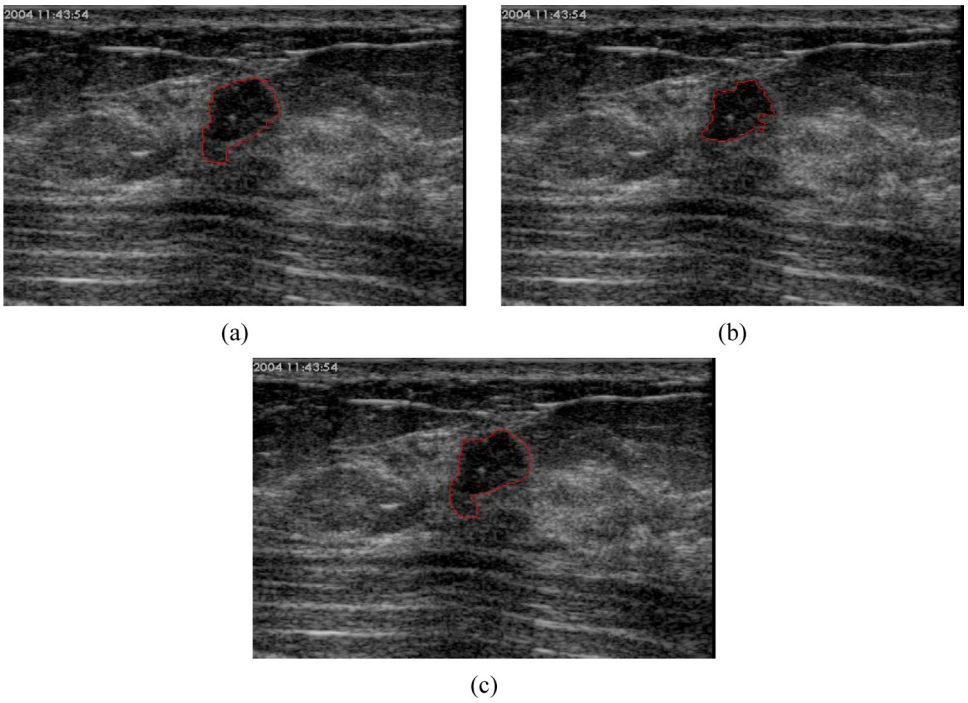

Fig. 4 – Example of tumor segmentation with different methods: (a) result by NSSLS, (b) result by FCMLS, and (c) radiologist's result.

where $H(x, y)$ is the homogeneity value at (x, y), which is depicted as the filtering result with the texture energy measurement (TEM) filter [23]. $Gd_h(x, y)$ is the gradient magnitude value on $H(x, y)$.

Then, a similarity value is calculated to identify the degree to the ideal object under different conditions:

$$S_{C_g}(P(x,y), A^*) = \frac{T_{C_g}(x,y)T_{C_g}(A^*) + I_{C_g}(x,y)I_{C_g}(A^*) + F_{C_g}(x,y)F_{C_g}(A^*)}{\sqrt{T^2_{C_g}(x,y) + I^2_{C_g}(x,y) + F^2_{C_g}(x,y)} \times \sqrt{T^2_{C_g}(A^*) + I^2_{C_g}(A^*) + F^2_{C_g}(A^*)}} \quad (13)$$

$$S_{C_m}(P(x,y), A^*) = \frac{T_{C_m}(x,y)T_{C_m}(A^*) + I_{C_m}(x,y)I_{C_m}(A^*) + F_{C_m}(x,y)F_{C_m}(A^*)}{\sqrt{T^2_{C_m}(x,y) + I^2_{C_m}(x,y) + F^2_{C_m}(x,y)} \times \sqrt{T^2_{C_m}(A^*) + I^2_{C_m}(A^*) + F^2_{C_m}(A^*)}} \quad (14)$$

$$S_{C_h}(P(x,y), A^*) = \frac{T_{C_h}(x,y)T_{C_h}(A^*) + I_{C_h}(x,y)I_{C_h}(A^*) + F_{C_h}(x,y)F_{C_h}(A^*)}{\sqrt{T^2_{C_h}(x,y) + I^2_{C_h}(x,y) + F^2_{C_h}(x,y)} \times \sqrt{T^2_{C_h}(A^*) + I^2_{C_h}(A^*) + F^2_{C_h}(A^*)}} \quad (15)$$

The value of A^* under three conditions are same as: $\{T^*_{C_j}(A_i), I^*_{C_j}(A_i), F^*_{C_j}(A_i)\}/A^*_i = \{1, 0, 0\}/A^*$.

The final single value of S_{C_g}, S_{C_m} and S_{C_h} is defined as:

$$\mathrm{NSF}(x,y) = \frac{S_{C_g}(x,y) + S_{C_m}(x,y) + S_{C_h}(x,y)}{3} \quad (16)$$

2.2. *Level set*

Level set method has been proposed [24], and applied for image segmentation [25]. The level set based image segmentation methods was usually grouped into two ways: edge and region based methods. The edge based model tries to find a curve with the maximum edge indicator value which can minimize the energy function $J(C)$ [26]:

$$J(C) = \int |C'(s)|\, g(\mathrm{Im}(C(s)))ds \quad (17)$$

where $g()$ is an edge indicator function, C is the boundary, and it can be represented implicitly as the zero level set of a true positive function $\phi : \Omega \to R$, Ω is the domain of image. The evolution equation of boundary C can be derived as:

$$\begin{cases} \dfrac{\partial \phi}{\partial t} = |\nabla \phi| \left(\mathrm{div}\left(g(\mathrm{Im}) \dfrac{\nabla \phi}{|\nabla \phi|} \right) + v(\mathrm{Im}) \right) \\ \phi(0, x, y) = \phi_0(x, y) \quad \text{in } \Omega \end{cases} \quad (18)$$

where $v()$ is a term for increasing the evolution speed to reach the boundary.

The region based model uses the inside and outside mean values to calculate the energy function [27]:

$$F(C, c_1, c_2) = \mu_1 L(C) + \mu_2 S(C) + \lambda_1 \int_{S_1} |\mathrm{Im} - c_1|^2 dS_1 + \lambda_2 \int_{S_2} |\mathrm{Im} - c_2|^2\, dS_2 \quad (19)$$

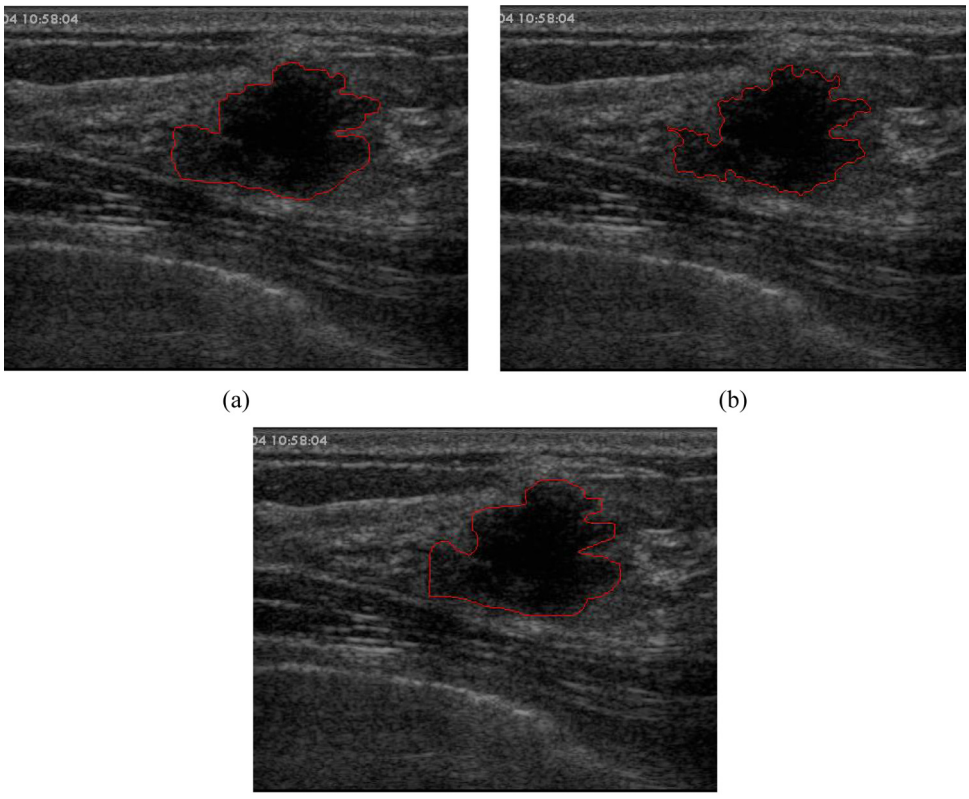

Fig. 5 – Example of tumor segmentation with different methods: (a) result by NSSLS, (b) result by FCMLS, and (c) radiologist's result.

where c_1 and c_2 are the mean intensities of the regions inside and outside the boundary C, respectively. L and S are the length of C and the area inside C. S_1 and S_2 are the region inside and outside of C, respectively. The associated level set flow can be represented as:

$$\begin{cases} \dfrac{\partial \phi}{\partial t} = \delta(\phi)\left[\mu \operatorname{div}\left(\dfrac{\nabla \phi}{|\nabla \phi|}\right) - \upsilon - \lambda_1(\mathrm{Im} - c_1)^2 + \lambda_2(\mathrm{Im} - c_2)^2\right] \\ \phi(0, x, y) = \phi_0(x, y) \\ \dfrac{\delta(\phi)}{|\nabla \phi|}\dfrac{\partial \phi}{\partial n} = 0 \end{cases} \tag{20}$$

where $\delta()$ is the Dirac function, and n denotes the exterior normal to the boundary $\partial\Omega$. div() is the divergence function on the image.

Usually, edge based approaches often suffer from noise, especially, when the image has a low signal/noise ratio; while the region based approaches are more adaptive to noise or vanishing boundaries due to considering the entire information of the regions to build an energy function.

2.3. *BUS image segmentation based on neutrosophic similarity score and level set*

A novel BUS segmentation method based on neutrosophic similarity score and level set algorithm (NSSLS) is proposed to

Table 1 – The performance of computer segmentation with reference to an experienced radiologist's manually drawn boundaries for the FCMLS, INSS and the NSSLS methods.

Method		POA (%)	Hdist (mm)	AvgDist (mm)
FCMLS		69.9 ± 11.9	34.9 ± 45.6	10.3 ± 27.7
NSSLS		82.3 ± 5.6	24.1 ± 17.0	4.8 ± 2.5
INSS		79.4 ± 2.6	30.4 ± 8.3	6·7 ± 3.4
p-Value	NSSLS vs FCMLS	$<10^{-12}$	0.037	0.044
	NSSLS vs INSS	0.023	0.040	0.048

The *p*-values of the differences between the three methods are estimated by the two-tailed *t*-test.

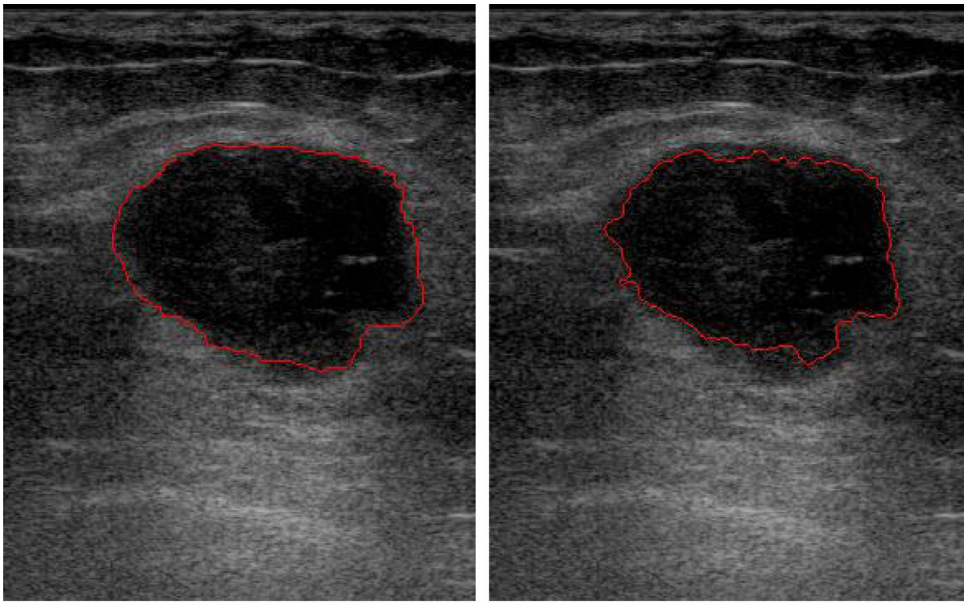

Fig. 6 – Example of tumor segmentation with different method in a benign case: (a) result by NSSLS, (b) result by FCMLS, and (c) radiologist's result.

Table 2 – The performance of computer segmentation with reference to an experienced radiologist's manually drawn boundaries for the INLS and the EMM method: with versus without extensive lung diseases.

	Method	POA (%)	Hdist (mm)	AvgDist (mm)
Malign cases	FCMLS	72.5 ± 8.5	32.6 ± 24.2	7.7 ± 4.0
	NSSLS	83.4 ± 5.7	22.4 ± 14.4	4.3 ± 1.8
p-Value		$<10^{-10}$	0.049	$<10^{-5}$
Benign cases	FCMLS	66.9 ± 14.4	37.5 ± 31.8	13.4 ± 10.4
	NSSLS	81.0 ± 5.3	25.7 ± 19.1	5.2 ± 3.0
p-Value		$<10^{-4}$	0.049	0.048
Malign vs benign cases *p*-value	FCMLS	0.075	0.431	0.160
	NSSLS	0.065	0.681	0.441

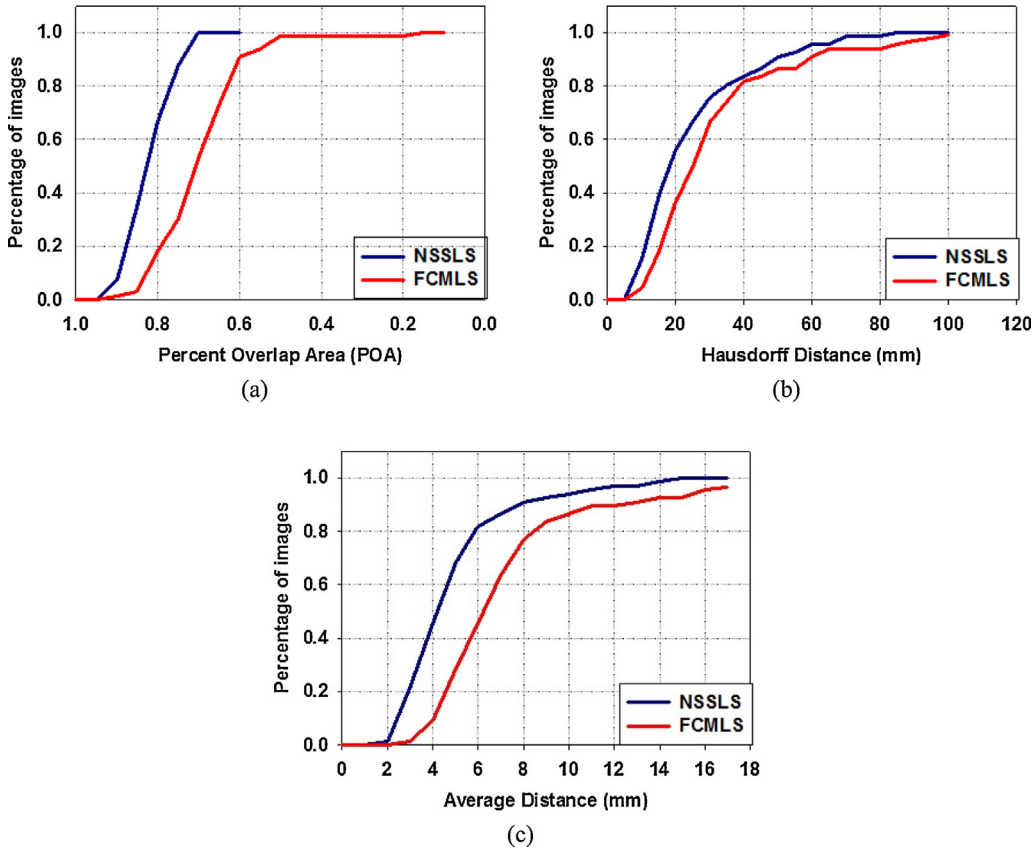

Fig. 7 – Cumulative percentage relative to the 66 images with radiologist's manually drawn tumor regions as reference standards, (a) having percent overlap area (POA) between the computer-segmented tumor region and the reference standard greater than a certain value, and having (b) Hausdorff distance measure and (c) average Euclidean distance measure between the computer-segmented boundary and the reference standard smaller than a certain value.

segment the tumors in BUS image. The image is interpreted using NSS under three conditions, and the boundary of tumor region is extracted using the level set active contour algorithm based on the region model. The energy function is defined using the NSS values.

$$F(C, c_1, c_2) = \mu_1 L(C) + \mu_2 S(C) + \lambda_1 \int_{S_1} |T' - c_1|^2 dS_1 + \lambda_2 \int_{S_2} |T' - c_2|^2 dS_2 \quad (21)$$

The flowchart of the proposed method can be seen in Fig. 1.

3. Experimental results and discussions

We have tested the proposed algorithm using different clinical images, and compared its performance with those of newly developed algorithms. In the experiments, we compare the NSSLS method with a published method based on fuzzy c-means and level set (FCMLS) [28].

The proposed algorithm is tested using a number of clinical BUS images provided by the Second Affiliated Hospital of Harbin Medical University, Harbin, China. Approved by IRB in hospital, we collected the images using a VIVID 7 (GE, Horten, Norway) with a 4–5 MHz linear probe, and captured directly from the video signals. The tested database consists of 66 images and a single lesion is in each image. All cases were confirmed by biopsy or operation, and experienced radiologists outlined the lesions as the ground truth.

Figs. 2–6 show five representative examples of the segmented tumor regions by two methods. These examples are from different subcategories of benign and malign diseases, respectively. They include most cases of breast cancer in our collection and can represent the distribution of the case in our data set. From the segmentation results, we can see clearly the proposed method can segment the tumor completely and smoothly and well preserve the useful information for diagnosis such as edge and boundary on all examples.

The tumor boundaries identified by the different methods are superimposed on the original image using red lines. From the comparison results, we can see clearly that the results by NSSLS method are more accurate and closer to the ground truth than those by FCMLS method.

To evaluate the segmentation results quantitatively, three measurements are employed to compare the segmentation results with the experienced radiologists' manual segmentation results. The tumor boundaries manually outlined by an experienced radiologist were used as the reference standard for the performance evaluation of tumor segmentation

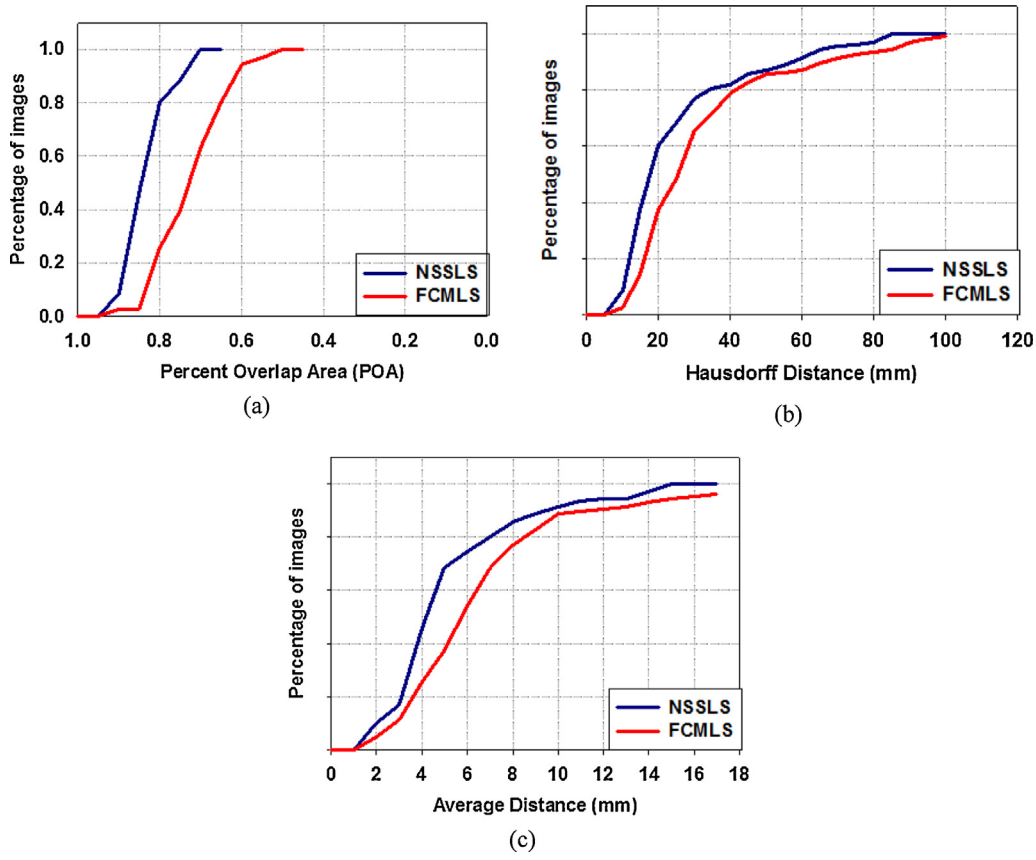

Fig. 8 – Cumulative percentage of cases relative to the 35 malign cases with radiologist's hand-drawn tumor regions as reference standards, (a) having percent overlap area (POA) between the computer-segmented tumor region and the reference standard greater than a certain value, and having (b) Hausdorff distance measure and (c) average Euclidean distance measure between the computer-segmented boundary and the reference standard smaller than a certain value.

algorithm. Let $C = \{c_1, c_2, \ldots, c_p\}$ be the computer-identified tumor boundary that contains p singly-connected points, and $R = \{r_1, r_2, \ldots, r_q\}$ be radiologist's manually outlined tumor boundary that contains q singly-connected points. The Euclidean distance between a computer-identified tumor boundary point c_i and a reference standard point r_j is $\mathrm{Dist}(c_i, r_j)$, or equivalently, $\mathrm{Dist}(r_j, c_i)$. The accuracy of tumor segmentation is evaluated by three performance metrics:

(1) Percent overlap area (POA):

$$\mathrm{POA}(C, A) = \frac{A_C \cap A_R}{A_C \cup A_R} \tag{22}$$

where A_C and A_R are the computer segmented tumor area and the reference standard tumor area enclosed by the boundaries C and R. $\cup$ and $\cap$ are the union and intersection of two sets, respectively.

(2) Hausdorff distance between the boundaries C and R (Hdist):

$$\mathrm{Hdist} = \max\left\{\max_{c_i \in C}\left\{\max_{r_j \in R}\{\mathrm{Dist}(c_i, r_j)\}\right\}, \max_{r_j \in R}\left\{\max_{c_i \in C}\{\mathrm{Dist}(r_j, c_i)\}\right\}\right\} \tag{23}$$

(3) Average distance between the boundaries C and R (AvgDist):

$$\mathrm{AvgDist} = \frac{1}{2}\left(\frac{1}{p}\sum_{i=1}^{p}\min_{r_i \in R}\{\mathrm{Dist}(c_i, r_j)\} + \frac{1}{q}\sum_{j=1}^{q}\min_{c_i \in C}\{\mathrm{Dist}(r_j, c_i)\}\right) \tag{24}$$

The distance measures are calculated in units of mm.

Total 66 images were selected from the 66 cases and the tumor boundaries were manually outlined, which were used as the reference standard for performance evaluation. The 66 representative cases include most categories of breast cancer in our data set. In comparison with radiologist's manual outlines, the performance metrics (POA, Hdist and AvgDist) were calculated on the corresponding images and the mean and standard deviation were computed over the 66 images. As shown in Table 1, the mean and standard deviation of the POA, Hdist and AvgDist were improved from $69.9 \pm 11.9\%$, 34.9 ± 45.6 mm, and 10.3 ± 27.7 mm using FCMLS to $82.3 \pm 5.6\%$, 24.1 ± 17.0 mm, and 4.8 ± 2.5 mm using NSSLS, respectively. The improvement is statistically significant ($p < 0.05$) for each performance metric by two-tailed t-test.

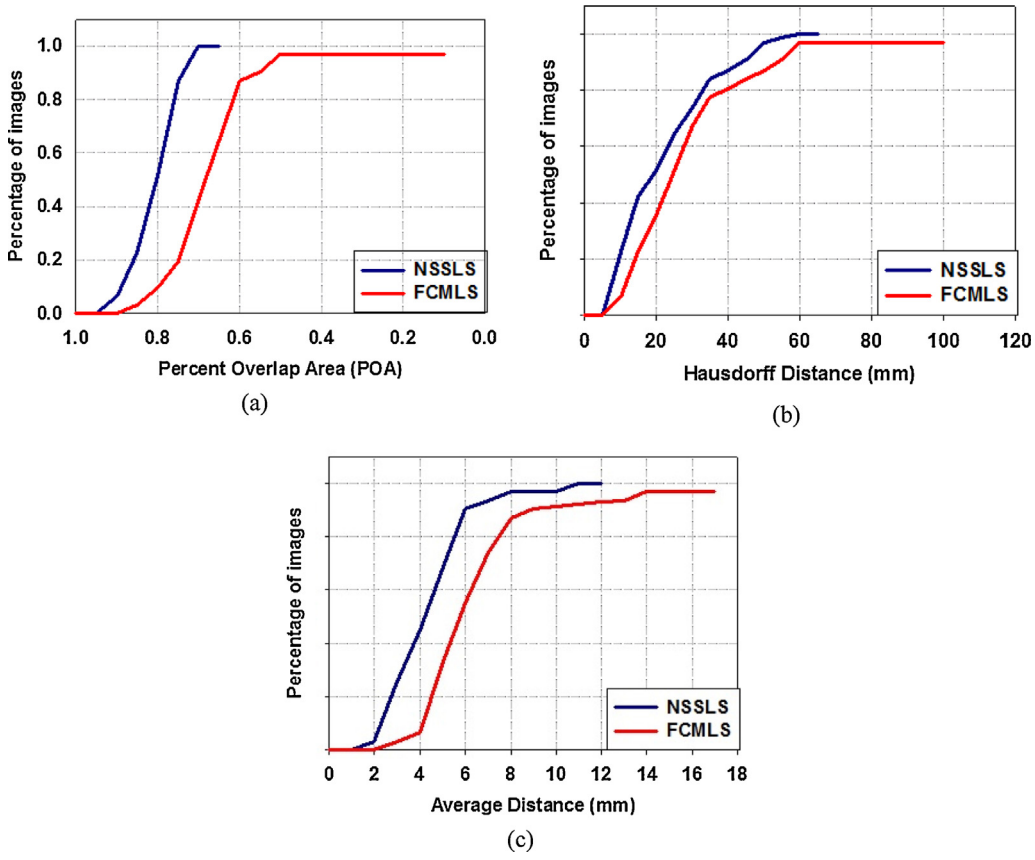

Fig. 9 – Cumulative percentage of cases relative to the 31 benign cases with radiologist's hand-drawn tumor regions as reference standards, (a) having percent overlap area (POA) between the computer-segmented tumor region and the reference standard greater than a certain value, and having (b) Hausdorff distance measure and (c) average Euclidean distance measure between the computer-segmented boundary and the reference standard smaller than a certain value.

We also compare the proposed method with the newly published segmentation algorithm based on interval neutrosophic set (INSS) [29], and the results are also listed in Table 1. The mean and standard deviation of the POA, Hdist and AvgDist of INSS are $79.4 \pm 2.6\%$, 31.4 ± 8.3 mm, and 6.7 ± 3.4 mm using FCMLS, which are worse than those of NSSLS method. The improvements from INSS to NSSLS are also significant ($p < 0.05$) for each metric by two-tailed t-test.

Fig. 7(a)–(c) shows the cumulative percentage of cases having POA greater than a certain value and Hdist and AvgDist smaller than a certain value on the results of FCMLS and NSSLS, respectively. From the results of NSSLS, it shows that 90.3% cases in the computer-segmented tumor had POA $\geq$ 85%, and that 82.1% and 99.8% cases in the computer-segmented tumor boundaries had Hdist $\leq$ 25 mm, and AvgDist $\leq$ 5 mm, respectively.

To test the segmentation performance for the malign and benign cases, the 66 test cases were separated into two groups: 35 malign cases and 31 benign cases. Table 2 shows the segmentation results for the different cases using the FCMLS and the NSSLS method. For both the FCMLS method and the NSSLS method, the average POA was higher and the Hdist and AvgDist were smaller for the malign cases than those benign cases. For all cases, all three performance measures by the NSSLS method were significantly ($p < 0.05$) better than those by the FCMLS method.

Comparing the NSSLS method with the FCMLS method, the POA improved by 15% and 21.1% in the malign and benign cases, respectively, and the Hdist and AvgDist improved by 31.3% and 44.2% in the malign cases, and by 31.5% and 61.2% in the benign cases, respectively. Furthermore, comparing the performance in the malign and benign cases, the POA, Hdist, and AvgDist were degraded by only 2.9%, 14.7%, and 20.9%, respectively, by the NSSLS method, whereas they were degraded by 7.7%, 15.0% and 74.0%, respectively, by the FCMLS method.

The comparison demonstrates that the NSSLS method can achieve better performance on both the malign and benign cases than the FCMLS method, and the NSSLS method is more robust against different cases than the FCMLS method for all three-performance measures.

Figs. 8 and 9 show the cumulative percentage of slices having distance measurements less than a certain value. The results show that both the FCMLS and NSSLS methods achieved better performance for the malign cases than the benign cases. For each metric, the NSSLS method reaches higher percentage than the FCMLS method. From the experiments and evaluation on clinical images, we can draw a

conclusion that the NSLS method is feasible to segment tumor in the BUS images.

4. Conclusions

This study demonstrated that our new NSSLS method utilizing neutrosophic similarity score for the indeterminate information on the breast image and fusion with level set method improved the tumor segmentation significantly, for both malign and benign cases with different tumor size and shape. Automated and accurate tumor segmentation is a fundamental step for many image analysis tasks and CAD applications in breast cancer detection and diagnosis, and the proposed method will find more application in these areas.

Conflict of interest

We declare that we have no financial and personal relationships with other people or organizations that can inappropriately influence our work, there is no professional or other personal interest of any nature or kind in any product, service and/or company that could be construed as influencing the position presented in, or the review of, the manuscript.

Acknowledgment

This work is supported by NSFC Grant 81071216 and 81271647.

REFERENCES

[1] R. Siegel, J. Ma, Z. Zou, A. Jemal, Cancer statistics, 2014, CA Cancer J. Clin. 64 (January–February (1)) (2014) 9–29.
[2] A. C. Society, Cancer Facts & Figures 2014, American Cancer Society, Atlanta, 2014.
[3] S.K. Moore, Better breast cancer detection, Spectr. IEEE 38 (5) (2001) 50–54.
[4] B. Liu, H.D. Cheng, J. Huang, J. Tian, X. Tang, J. Liu, Fully automatic and segmentation-robust classification of breast tumors based on local texture analysis of ultrasound images, Pattern Recognit. 43 (January (1)) (2010) 280–298.
[5] H.D. Cheng, J. Shan, W. Ju, Y. Guo, L. Zhang, Automated breast cancer detection and classification using ultrasound images: a survey, Pattern Recognit. 43 (1) (2010) 299–317.
[6] H.D. Cheng, X.H. Jiang, Y. Sun, J. Wang, Color image segmentation: advances and prospects, Pattern Recognit. 34 (12) (2001) 2259–2281.
[7] M. Kass, A. Witkin, D. Terzopoulos, Snakes: active contour models, Int. J. Comput. Vis. 1 (4) (1988) 321–331.
[8] R.-F. Chang, W.-J. Wu, W.K. Moon, W.-M. Chen, W. Lee, D.-R. Chen, Segmentation of breast tumor in three-dimensional ultrasound images using three-dimensional discrete active contour model, Ultrasound Med. Biol. 29 (November (11)) (2003) 1571–1581.
[9] J.A. Noble, D. Boukerroui, Ultrasound image segmentation: a survey, IEEE Trans. Med. Imaging 25 (8) (2006) 987–1010.
[10] A. Madabhushi, D.N. Metaxas, Combining low-, high-level and empirical domain knowledge for automated segmentation of ultrasonic breast lesions, IEEE Trans. Med. Imaging 22 (2) (2003) 155–169.
[11] B. Liu, H.D. Cheng, J. Huang, J. Tian, J. Liu, X. Tang, Automated segmentation of ultrasonic breast lesions using statistical texture classification and active contour based on probability distance, Ultrasound Med. Biol. 35 (August (8)) (2009) 1309–1324.
[12] S. Selvan, S. Shenbagadevi, Automatic seed point selection in ultrasound echography images of breast using texture features, Biocybernet. Biomed. Eng. (October) (2014) (online).
[13] L.A. Christopher, E.J. Delp, C.R. Meyer, P.L. Carson, 3-D Bayesian ultrasound breast image segmentation using the EM/MPM algorithm, in: Proceedings, 2002 IEEE International Symposium on Biomedical Imaging, 2002, pp. 86–89.
[14] G. Xiao, M. Brady, J.A. Noble, Y. Zhang, Segmentation of ultrasound B-mode images with intensity inhomogeneity correction, IEEE Trans. Med. Imaging 21 (1) (2002) 48–57.
[15] Y.L. Huang, D.R. Chen, Watershed segmentation for breast tumor in 2-D sonography, Ultrasound Med. Biol. 30 (May (5)) (2004) 625–632.
[16] D.-R. Chen, R.-F. Chang, W.-J. Kuo, M.-C.Y. Chen, U.-L. Huang, Diagnosis of breast tumors with sonographic texture analysis using wavelet transform and neural networks, Ultrasound Med. Biol. 28 (10) (2002) 1301–1310.
[17] J. Shan, Y. Wang, H.D. Cheng, Completely automatic segmentation for breast ultrasound using multiple-domain features, in: 2010 17th IEEE International Conference on Image Processing (ICIP), 26–29 September, 2010, pp. 1713–1716, http://dx.doi.org/10.1109/ICIP.2010.5652626.
[18] Q. Huang, F. Yang, L. Liu, X. Li, Automatic segmentation of breast lesions for interaction in ultrasonic computer-aided diagnosis, Inf. Sci. (2014) (online).
[19] J. Peng, P. Jingliang, Z. Guoquan, C. Erkang, V. Megalooikonomou, L. Haibin, Learning-based automatic breast tumor detection and segmentation in ultrasound images, in: 2012 9th IEEE International Symposium on Biomedical Imaging (ISBI), 2012, pp. 1587–1590.
[20] D.C. Pereira, R.P. Ramos, M.Z. do Nascimento, Segmentation and detection of breast cancer in mammograms combining wavelet analysis and genetic algorithm, Comput. Methods Programs Biomed. 114 (1) (2014) 88–101.
[21] X. Zhang, F. Jia, S. Luo, G. Liu, Q. Hu, A marker-based watershed method for X-ray image segmentation, Comput. Methods Programs Biomed. 113 (3) (2014) 894–903.
[22] J. Ye, Multicriteria decision-making method using the correlation coefficient under single-valued neutrosophic environment, Int. J. Gen. Syst. 42 (May (4)) (2013) 386–394.
[23] Y. Guo, A. Sengur, A novel color image segmentation approach based on neutrosophic set and modified fuzzy c-means, Circuits Syst. Signal Process. 32 (August (4)) (2013) 1699–1723.
[24] S. Osher, J.A. Sethian, Fronts propagating with curvature-dependent speed: algorithms based on Hamilton–Jacobi formulations, J. Comput. Phys. 79 (November (1)) (1988) 12–49.
[25] R. Malladi, J.A. Sethian, B.C. Vemuri, Shape modeling with front propagation: a level set approach, IEEE Trans. Pattern Anal. Mach. Intell. 17 (2) (1995) 158–175.
[26] V. Caselles, R. Kimmel, G. Sapiro, Geodesic active contours, Int. J. Comput. Vis. 22 (February (1)) (1997) 61–79.
[27] T.F. Chan, L.A. Vese, Active contours without edges, IEEE Trans. Image Process. 10 (2) (2001) 266–277.
[28] S. Alipour, J. Shanbehzadeh, Fast automatic medical image segmentation based on spatial kernel fuzzy c-means on level set method, Mach. Vis. Appl. 25 (August (6)) (2014) 1469–1488.
[29] L. Zhang, M. Zhang, Segmentation of blurry images based on interval neutrosophic set, J. Inf. Comput. Sci. 12 (7) (2015) 2769–2777.